


The development and characterization of a CRISPR/Cas9-mediated PD-1 functional knockout rat as a tool to study idiosyncratic drug reactions

Tiffany Cho, Antonia Wierk, Marina Gertsenstein , Christopher E. Rodgers, Jack Uetrecht,* Jeffrey T. Henderson

Department of Pharmaceutical Sciences, Leslie Dan Faculty of Pharmacy, University of Toronto, Toronto, Ontario M5S 3M2, Canada

*To whom correspondence should be addressed at Department of Pharmaceutical Sciences, Leslie Dan Faculty of Pharmacy, University of Toronto, 144 College Street, Toronto, ON M5S 3M2, Canada. E-mail: jack.uetrecht@utoronto.ca.

Abstract

Idiosyncratic drug reactions are rare but serious adverse drug reactions unrelated to the known therapeutic properties of the drug and manifest in only a small percentage of the treated population. Animal models play an important role in advancing mechanistic studies examining idiosyncratic drug reactions. However, to be useful, they must possess similarities to those seen clinically. Although mice currently represent the dominant mammalian genetic model, rats are advantageous in many areas of pharmacologic study where their physiology can be examined in greater detail and is more akin to that seen in humans. In the area of immunology, this includes autoimmune responses and susceptibility to diabetes, in which rats more accurately mimic disease states in humans compared with mice. For example, oral nevirapine treatment can induce an immune-mediated skin rash in humans and rats, but not in mice due to the absence of the sulfotransferase required to form reactive metabolites of nevirapine within the skin. Using CRISPR-mediated gene editing, we developed a modified line of transgenic rats in which a segment of IgG-like ectodomain containing the core PD-1 interaction motif containing the native ligand and therapeutic antibody domain in exon 2 was deleted. Removal of this region critical for mediating PD-1/PD-L1 interactions resulted in animals with an increased immune response resulting in liver injury when treated with amodiaquine.

Keywords: idiosyncratic drug reactions; adverse drug reactions; idiosyncratic drug-induced liver injury; amodiaquine; immune tolerance; PD-1; animal models.

Idiosyncratic drug reactions (IDRs) are adverse events unrelated to the therapeutic actions of the drug that do not occur in most patients treated with a drug. Currently, there exists compelling evidence that most IDRs are immune-mediated, and there is additional circumstantial evidence to indicate that most IDRs are caused by reactive metabolites of the drug, which can act as haptens to modify proteins and initiate an immune response (Cho and Uetrecht, 2017; Jee et al., 2021; Sernoskie et al., 2021). The entirety of factors that may make an individual susceptible to IDRs is unknown. However, features such as the presence of specific HLA and/or T cell receptor combinations with affinity toward unique protein/peptide epitopes modified by the drug in question appear to play a role (Daly and Day, 2009). Although most IDRs are mild and may even resolve without additional intervention during continued drug treatment, some IDRs are severe and capable of inducing progressive cellular injury despite discontinuation of drug treatment. In some cases, this can ultimately result in permanent injury and even death (Pirmohamed et al., 2002). Due to their unpredictable nature, serious IDRs are usually not detected until late in phase clinical trials or even following drug approval. Such factors provide a significant risk for failure in drug development, the addition of drug labeling precautions, or market withdrawal. Based on their heterogeneous nature, there is currently no reliable preclinical or clinical

predictor to screen drugs or drug candidates for their potential to cause IDRs. In the event, a given IDR is immune-mediated, the complexity of the immune system precludes convenient *in vitro* assays that can fully assess the *in vivo* risk. Thus, as in other areas of biomedical investigation, animal models comprise an essential tool to evaluate the risk profile of IDRs.

It has been suggested that the unique tolerizing effects of the liver, which regulate local and systemic tolerance to self- and foreign antigens may play a role in preventing most individuals from developing a given IDR (Tiegs and Lohse, 2010). This effect is attributed to specialized resident cells including dendritic cells, liver sinusoidal endothelial cells, Kupffer cells, and hepatic stellate cells that act via the production of anti-inflammatory signaling agents such as IL-10 and TGF- β as well as by the expression of negative co-stimulator for T cell activation: programmed cell death ligand-1 (PD-L1). In many cases, IDRs appear to involve reactive metabolites generated by the liver (Cho and Uetrecht, 2017). It may be possible to better assess the potential of reactive metabolites to cause IDRs by modifying mechanisms of immunologic tolerance (Uetrecht and Kaplowitz, 2015). In cancer treatment, modification of immune function has been explored using immune checkpoint inhibitors such as programmed cell death-1 (PD-1) and cytotoxic T lymphocyte-associated protein 4 (CTLA-4), which act in inhibiting the immune response and play important

roles in regulating T cell activation (Buchbinder and Desai, 2016; Parry et al., 2005). A similar inhibitory role has been observed in PD-1-deficient mice in which loss of PD-1 triggers an enhancement of autoimmunity whose features and severity differ depending upon their genetic background (Nishimura and Honjo, 2001; Nishimura et al., 1999). Similarly, mutations of PD-1 in humans are associated with autoimmune disorders including systemic lupus erythematosus, diabetes, multiple sclerosis, rheumatoid arthritis, and Grave's disease (Gianchecchi et al., 2013).

With respect to the effects of immune checkpoint inhibitors on IDRs, we have previously observed that an application of anti-CTLA-4 antisera in PD-1^{-/-} mice unmasked the ability of certain drugs such as amodiaquine to cause idiosyncratic drug-induced liver injury (Mak and Uetrecht, 2015a; Metushi et al., 2015). However, the use of such immune-modified mice is not suitable for the investigation of all drugs. For example, in contrast to rats, mice lack the dermal sulfotransferase responsible for the formation of the reactive metabolite of nevirapine known to cause skin rash in humans (Sharma et al., 2013). Similarly, mice are significantly more sensitive to the neurological effects of clozapine than humans, making investigative IDR dosing studies in this species difficult. For these reasons, in addition to their more well-studied physiology and the enhanced behavioral readouts, rats represent an improved system over mice for examining several features of idiosyncratic drug reactivity (Iannaccone and Jacob, 2009). One traditional advantage of mice over rats as experimental models in past decades has been both the completeness of their genomic sequencing and availability of genetic resources required to perform targeted (homologous) recombination in mouse embryonic stem (ES) cells leading to the generation of genetically modified mice (Bouabe and Okkenhaug, 2013; Bryda, 2013). However, given the dramatic growth in the rat genome coverage in the past 20 years and the introduction of CRISPR-mediated gene targeting, the traditional advantages of murine systems have begun to equalize (Shao et al., 2014). Thus, in order to better understand the mechanism underlying drug-induced IDRs in the present study, we set out to develop an appropriate model system in rats to examine this process following the modification of immune checkpoints. CRISPR/Cas9-mediated genome editing was used to produce a phenotypically similar model to the PD-1-deficient mouse model. The rat PD-1 gene was modified such that ectodomain residues known to be critical for PD-1/PD-L1 interactions (and function-modifying anti-PD-1 antisera such as pembrolizumab) as previously identified from crystallographic studies were deleted in-frame (Horita et al., 2016). Such modification retained the C-terminal half of the immunoglobulin (Ig)G-like ectodomain, the transmembrane domain, and intracellular signaling components of PD-1, allowing direct and specific assessment of the influence of the PD-1/PD-L1 contact interaction domain *in vivo*.

Materials and methods

Animal procedures

CrI:CD Sprague Dawley (SD) rats were purchased from Charles River Laboratories (Montreal, QC, Canada) and maintained in the Canadian Council on Animal Care (CCAC)-accredited animal facility at the Hospital for Sick Children in individually ventilated units (Allentown; Allentown, New Jersey) on a 12-h light-dark cycle (6:00 AM–6:00 PM). Food and water were provided *ad libitum*. Fertile and vasectomized males were housed individually, with female SD rats utilized 1 week following acclimatization. Embryo manipulations were performed by the Model Production Core at

The Centre for Phenogenomics (TCP). For experiments, female and male rats were 8–12 weeks of age (250–300 g for females, 300–400 g for males). All Animal Use Protocols have been reviewed and approved by the Institutional Animal Care Committees and procedures followed CCAC guidelines contained in the Guide to Care and Use of Experimental Animals, Volume 1, second edition and CCAC Guidelines on Transgenic Animals (CCAC, 2020).

Six-to-seven-week-old SD females were injected subcutaneously with 40 µg of luteinizing-hormone-releasing hormone agonist (L4513; Sigma-Aldrich, St Louis, Missouri) between 9:00 and 10:00 AM to synchronize estrus 4 days before mating with vasectomized males to produce pseudopregnant recipients (Filipiak and Saunders, 2006). Two days before mating with fertile males, 4–5-week-old SD females were injected intraperitoneally with 20 IU of pregnant mare's serum gonadotropin (HOR-272; ProSpec, Ness-Ziona, Israel) at 8:00–9:30 AM followed 48 h later with 30 IU of human chorionic gonadotropin (hCG) (230734; EMD Millipore, Burlington, Massachusetts) then mated overnight with proven SD male breeders (Filipiak and Saunders, 2006). Females were checked the next morning for the presence of a vaginal plug. Oviducts were dissected approximately 22 h post-hCG and cumulus oocytes were released into M2 medium (ZFM2-100; Zenith Biotech) and treated with 0.3 mg/ml hyaluronidase (H4272; Sigma-Aldrich) as described previously (Behringer et al., 2014). Fertilized embryos were kept at 37°C, 6% CO₂ in microdrops of KSOM media with amino acids (ZEKS-050; Zenith Biotech) covered by embryo-tested paraffin oil (ZPOL-50; Zenith Biotech) prior to pronuclear microinjection, which was performed as described previously (Behringer et al., 2014). Briefly, RNP complexes (see below) were injected into approximately 100 pronuclei using glass capillaries with inner filament manufactured in-house or purchased from Biomedical Instruments (<http://www.biomedical-instruments.com/>) with a tip diameter of approximately 1.2 µm. An Eppendorf FemtoJet 4i injector was set to constant flow. Microinjections were performed under 200–250× magnification on a Leica inverted microscope with Nomarski optics using Leica micromanipulators. Viable microinjected embryos were subsequently transferred into the oviducts of 0.5-dpc pseudopregnant SD recipients as described (Behringer et al., 2014).

PD-1 gene modification

Guide RNA sequences were constructed using the SD (*Rattus norvegicus*) genomic database at the National Center for Biotechnology Information (NCBI) and *Ensembl* to target the desired exon sequences for PDCD1 (also known as PD-1 or programmed cell death 1—NC005108.4). Identified sequence guides were also assessed using <http://crispr.mit.edu> and <http://chop-chop.cbu.uib.no>. DNA oligos were synthesized by Integrated DNA Technologies (IDT; Coralville, Iowa) with sequence pairs cloned into vector pX459v2 (Addgene, 62988; Cambridge, Massachusetts) at the BbsI site, with single-guide RNAs (sgRNAs) expressed under the U6 promoter. pX459v2 also expresses a FLAG-tagged nuclearly localized *S. pyogenes* Cas9 fused in-frame via T2A cleavage sequence to a puromycin resistance marker for selection. All targeted clones obtained were confirmed by sequencing.

sgRNAs were synthesized as described previously (Gertsenstein and Nutter, 2018). Briefly, templates for *in vitro* synthesis of sgRNAs were produced by high fidelity PCR using KAPA HiFi polymerase (KK2601; Kapa Biosystems, Wilmington, Massachusetts), transcribed with MEGAscript T7 Transcription Kit (AM1354; Life Technologies, Carlsbad, California), then purified with MEGAclear Transcription Clean-

Up Kit (AM1908; Life Technologies). Purified sgRNAs were analyzed on an Agilent Bioanalyzer at The Centre for Applied Genomics (TCAG) at The Hospital for Sick Children (Toronto, ON, Canada) to assess integrity. Concentration was determined by Qubit with the Broad Range RNA Assay Kit (Q10211; Thermo Fisher). Pronuclear microinjection mixes were prepared as described (Gertsenstein and Nutter, 2018) consisting of 20 ng/ μ l Cas9 mRNA (A23978; Life Technologies) and 10 ng/ μ l of each desired sgRNA or sgRNA pool in microinjection buffer (10 mM Tris, 0.1 mM EDTA). All genomic clones obtained were confirmed by sequencing.

Animal genotyping

DNA samples for genotyping were obtained from ear clips (approximately 2 mm) at 3 weeks of age and stored at -20°C if not used immediately. Samples were resuspended in digestion buffer (100 mM NaCl, 50 mM Tris-HCl pH 8.0, 2 mM EDTA pH 8.0, 0.5% SDS) with 10 mg/ml proteinase K (PRK403.100; BioShop, Burlington, ON, Canada) and subsequently incubated at 65°C for 2.5 h, with DNA precipitated and resuspended in 100 μ l sterile distilled water. HotStart genotyping (KK7351; Kapa Biosystems) was performed according to the manufacturer's instructions using a Chromo4 RT Thermo Cycler (Bio-Rad; Hercules, California). Amplification was conducted at 95°C for 3 min followed by 35 cycles (95°C for 15 s, 60°C for 15 s, and 72°C for 20 s) with a final extension phase at 72°C for 1 min. Sanger sequencing was performed at TCAG (Toronto, ON, Canada), with results visualized using the ApE Plasmid Editor (Wayne Davis; University of Utah, Salt Lake City, Utah).

Western blotting and protein staining

Protein lysates were obtained from isolated whole thymus at endpoint, where samples were passed through a 70- μ m strainer with 500 μ l $1\times$ RIPA buffer (20 mM Tris-HCl pH 7.5, 150 mM NaCl, 1 mM Na_2EDTA , 1 mM EGTA, 1% NP-40, 1% sodium deoxycholate, 2.5 mM sodium pyrophosphate, 1 mM β -glycerophosphate, 1 mM sodium orthovanadate, 1 μ g/ml leupeptin) purchased from Cell Signaling Technology (Danvers, Massachusetts) and $1\times$ Protein Inhibitor Cocktail (PIC, P8340; Sigma-Aldrich). Cells were disrupted using the Bioruptor Plus sonication device (Diagenode; Seraing, Belgium) for 3 cycles (30 s on, 30 s off) and samples were subsequently incubated at 4°C for 30 min on a rotator (Cole-Parmer; Staffordshire, UK). Spleen samples from animals of the indicated genotype were dissociated using a Dounce homogenizer in 50 mM NaCl, 20 mM Tris-HCl (pH 7.5 at 25°C), and 0.1 mM EDTA with protein homogenate concentrations determined using Pierce BCA protein assay (23227; VWR). One hundred micrograms of protein mixtures were deglycosylated using NEB Deglycosylation Mix II (P6044S, New England Biolabs; Ipswich, Massachusetts) in a total volume of 20 μ l Denaturing Buffer. Following denaturation, samples were chilled on ice and centrifuged, followed by the addition of 5 μ l of $10\times$ Reaction Buffer, 5 μ l 10% NP40, and 15 μ l H_2O and incubation for 30 min at 25°C . Lysates were centrifuged at $12\ 000\times$ g and the protein concentration of the supernatant was determined using the Pierce BCA Protein Assay Kit (23225; Thermo Fisher). Fc-tagged purified rat PD-1 protein (PD1-R5253, ACROBiosystems; Newark, Delaware) was used as a positive control (4 μ g). A 10% Mini-PROTEAN TGX Precast Protein Gel (4561034; Bio-Rad) was used to resolve 50 μ g of protein lysate via sodium dodecyl sulfate-polyacrylamide gel electrophoresis (SDS/PAGE) with $1\times$ Pierce Lane Marker Reducing Sample Buffer. Using the Mini Trans-Blot Cell system (Bio-Rad), proteins were resolved at a constant 120 V and transferred to a

0.45- μ m nitrocellulose membrane (1620115; Bio-Rad) at a constant 25 W for 1.5 h. The membrane was blocked with 5% skim milk powder (SKI400; BioShop) + 0.1% Tween 20 (TWN510; BioShop) for 1 h and then incubated overnight with a primary rabbit polyclonal anti-rat PD-1/CD279 antibody (18106-1-AP, Proteintech; Rosemont, Illinois). The membrane was washed and incubated with goat anti-rabbit secondary antibody conjugated to horseradish peroxidase (ab6721; Abcam, Cambridge, UK) at room temperature for 2 h. After washing, bands were developed using the Clarity Max ECL Substrate (1705060; Bio-Rad) and visualized using the Bio-Rad ChemiDoc MP.

Amodiaquine treatment

Amodiaquine hydrochloride (IPCA Laboratories, Mumbai, India) was thoroughly mixed with Teklad global 18% rodent meal (2018; Harlan Laboratories; Indianapolis, Indiana) at a concentration of 0.2% (w/w). Care was taken in performing serial dilutions of drug-mixed food through vigorous mixing. Food and water were provided *ad libitum* to rats starting on day 0; control animals received regular rodent meal. Approximately 100 μ l of blood was collected weekly via the tail vein using a 23G needle, which was repeated for the duration of the experiment (up to 3 weeks). Serum aminotransferase (ALT) levels were examined as a biomarker of liver injury. Whole blood was collected in Microvette capillaries with clot activator additive (CB300; Sarstedt; Nümbrecht, Germany) and centrifuged for 5 min at $11\ 200\times$ g. Using the ALT Liquid Stable Reagent (Thermo Fisher), ALT activity levels were determined as per package instructions. Body weights were recorded together with liver, spleen, thymus, and inguinal lymph node tissue weights at necropsy. Rats were euthanized by CO_2 asphyxiation following 3 weeks of treatment.

Histology and immunohistochemistry

The distal segment of the left lateral lobe of the liver, spleen, inguinal lymph nodes, and thymus was collected at the indicated endpoints. All samples were fixed in 10% neutral buffered formalin (Sigma-Aldrich) for 1 h. Following rinsing in $1\times$ PBS, tissue samples were dehydrated in a series of ethanol and xylene baths, and then prepared for paraffin embedding following standard procedures. Samples were sectioned at 5 μ m, dewaxed, and stained with hematoxylin/eosin by standard procedures, or processed for immunohistochemistry as indicated below. Slides were dehydrated, mounted, and scanned using a Hamamatsu NanoZoomer 2.0 HT at $20\times$ (Hamamatsu Photonics; Shizuoka, Japan) at the Princess Margaret Hospital HistoCore and University of Toronto (Toronto, ON, Canada). Immunohistochemistry for PD-1 was performed by the HistoCore following dewaxing and removal of endogenous peroxidase activity; samples were washed and blocked in Histoblock solution containing 3% BSA, 20 mM MgCl_2 , and 0.3% Tween 20 in 10 mM PBS, pH 7.4, with additional 0.2% Triton X-100 and 5% goat serum. Primary antibody (anti-PD-1/CD279 Rabbit polyclonal, 18106-1-AP; Proteintech) was then applied in Histoblock at a 1:250 dilution for 1 h at room temperature. Following washing in primary diluent for 3 times at 5 min, sections were incubated in goat anti-rabbit horseradish peroxidase conjugate (Jackson 111-035-033) at 1:500 for 1 h at room temperature followed by washing in PBS 3 times at 5 min and mounted as described above.

Flow cytometry and reagents

Liver mononuclear cells were isolated by digestion of minced whole liver in digestion buffer ($1\times$ PBS, 0.05% Type IV collagenase from *Clostridium histolyticum* [C0130; Sigma-Aldrich], 1.25 mM

CaCl₂, 4 mM MgSO₄, 10 mM HEPES) for 30 min at 37°C. Spleen samples were similarly processed without prior digestion. Cells were subsequently strained through a 100-µm cell strainer in a solution of 2–5 ml anti-coagulant-citrate-dextrose (ACD) buffer (1× PBS, 0.5% fetal bovine serum [F2242; Sigma-Aldrich] with 0.6% citrate-dextrose solution [C3821; Sigma-Aldrich] in 10 mM HEPES) and centrifuged for 3 min at 30 × g at 4°C to remove cell clusters. The cell supernatant was then collected and centrifuged at 320 × g for 5 min at 4°C. The pellet was then resuspended in 2 ml RPMI buffer (1× RPMI-1640 medium [R0883; Sigma-Aldrich] 10% FBS, 10 mM HEPES) and layered onto a 30% Percoll gradient (14 ml 1× PBS, 6 ml Percoll [17-0891-01; GE Healthcare, Chicago, Illinois]). For isolation of peripheral blood mononuclear cells (PBMCs), whole blood was collected via cardiac puncture at the time of sacrifice and transferred into EDTA-coated collection tubes (368589; BD Biosciences, Franklin Lakes, New Jersey) (Higdon et al., 2016). Tubes were inverted and rinsed with isotonic PBS, then overlaid onto Ficoll Paque Plus (GE Healthcare) and centrifuged at 800 × g for 15 min at 4°C (brake off). The buffy coat was then collected and washed with 1× PBS. For all samples, single-cell pellets were resuspended in fluorescence-activated cell sorting (FACS) buffer (1× PBS, 1% FBS) and counted on a hemocytometer after staining with Trypan Blue (15250061; Thermo Fisher). Ten million live cells were plated per well.

All immuno incubations were conducted at room temperature in the dark. Cell centrifugation was performed at 650 × g for 5 min at 4°C. To reduce Fc receptor-mediated binding by antibodies of interest to FcγII receptor-bearing cells, purified mouse anti-rat CD32 (550270; BD Biosciences; 1:100 dilution) was preincubated with the cell suspension. Cells were characterized by staining with the following antisera: BV421-conjugated anti-CD3 (563948; 1:40 dilution), BV605-conjugated anti-CD45RA (740372; 1:100 dilution), BV650-conjugated anti-CD161 (744052; 1:100 dilution), BV711-conjugated anti-MHCII (RT1B) (744130; 1:100 dilution), BV786-conjugated anti-CD8 (740913; 1:133 dilution), and BUV395-conjugated anti-CD4 (740256; 1:133 dilution) from BD Biosciences; eFluor506-conjugated Fixable Viability Dye (65-0866-14; 1:100 dilution), FITC-conjugated anti-FOXP3 (11-5773-82; 1:50 dilution), PE-conjugated anti-CD279 (PD-1) (12-9985-82; 1:50 dilution), and PerCP-eFluor710-conjugated anti-CD25 (46-0390-82; 1:100 dilution) from Thermo Fisher; APC-conjugated anti-CD11b/c (201809; 1:40 dilution), APC/Cy7-conjugated CD45 (202216; 1:100 dilution), and PE/Cy7-conjugated anti-CD43 (202816; 1:40 dilution) from BioLegend (San Diego, California); and Alexa Fluor 700-conjugated anti-CD68 (MCA341A700; 1:50 dilution) from Bio-Rad. Helper T cells were denoted as CD3⁺CD4⁺, cytotoxic T cells as CD3⁺CD8⁺ cells, macrophages as CD68⁺CD11b⁺ cells, classical and nonclassical monocytes as CD11b⁺CD43⁻ and CD11b⁺CD43⁺ cells, respectively; T_{reg} cells as CD3⁺CD4⁺CD25⁺FOXP3⁺; NK cells as CD3⁻CD161⁺; NKT cells as CD3⁺CD161⁺; dendritic cells as CD11b/c⁺MHCII⁺; and B cells as CD3⁻CD45RA⁺. With respect to intracellular staining, the FOXP3 fixation/permeabilization solution (00-5523-00; Thermo Fisher) was used according to the manufacturer's instructions. Cells were counted on a BD LSR Fortessa X-20 Cell Analyzer (BD Biosciences) using FACSDiva for data acquisition. Data analysis was conducted on the FlowJo 10 software (Tree Star Inc., Ashland, Oregon). For flow cytometry analyses, cells were initially gated on singlets (FSC-H vs FSC-A), live cells, and then by the specific population. A minimum of 50 000 cells/sample were acquired for each analysis.

Behavioral tests

Behavioral assays were conducted between 12:00 PM and 5:00 PM. Room temperature, humidity, and white noise levels were held stable for all experiments. Researchers were blinded to the genotype of the animals during the collection and analysis of the data through the use of identification numbers. No animals were prematurely removed from the study, and no animals showed signs of thermal or mechanical injury during approved trial procedures.

Thermosensitivity

Animals were acclimated to the hot plate chamber (Model PE34 Series 8, IITC Life Science; Woodland Hills, California) for 5 min prior to testing. On the day of testing, a single animal was placed in the hot plate chamber at a baseline temperature of 35°C. After 10 s, the plate was heated at a rate of 3°C/min until the animal demonstrated nociceptive behavior involving either hind paw. Malmberg and Bannon (Bannon and Malmberg, 2007; Malmberg and Bannon, 2001) have indicated that forepaw activity is often associated with grooming and exploratory behaviors, with hind paw response more reliably associated with thermosensitivity reactions. The predominant response was hind paw licking with shaking or lifting; escape behaviors were rarely observed. The plate temperature evoking any of these reactions to either hind paw was identified as the noxious heat threshold for the animal. The time from placement on the hot plate until the first sign of discomfort was recorded. After recording the threshold temperature and latency to response, the plate was automatically cooled to 35°C, and the animal was immediately removed. A cut-off temperature of 50°C was used to prevent tissue damage.

Mechanosensitivity

Von Frey filaments from 0.008 to 300 g bending force (Stoelting; Dale Wood, Illinois) were utilized (filaments no. 6–14 were used) with baseline testing always beginning with filament no. 10. Testing procedures followed an increasing/decreasing pattern such that a positive response to a filament prompted subsequent use of a lower-valued filament whereas a negative response resulted in the next higher-value filament (greater force). The paw withdrawal threshold (PWT) was calculated based on the simplified up-down (SUDO) methodology previously described by Bonin et al. (2014). Rats were placed in acrylic chambers elevated above a wire mesh grid and allowed to acclimatize to the testing apparatus for 30 min. Once exploratory behavior ceased the von Frey filament was applied perpendicularly against the mid-plantar surface of the paw until the filament was distorted (slightly bent) and this was held in position for 3 s. A positive response was noted if the paw was briskly withdrawn upon the application of the filament. Flinching upon removal of the filament was also considered a positive response as described by Chaplan et al. (1994). Lack of paw withdrawal within the 3 s of filament application was marked as a negative response. Ambulation was considered an ambiguous response, and the stimulus was repeated. Each trial consisted of 5 perpendicular applications with one application every 5 s. After the first trial on the left paw, a second trial was conducted on the right paw after 10 min of acclimatization for a total of 2 trials per paw. Mechanical PWTs were obtained by averaging the 2 trials performed on each paw.

Statistical analyses

Data are presented as the mean ± standard error of the mean (SEM). One-way or 2-way analysis of variance (ANOVA) followed

by Tukey's post hoc test was used to assess for statistical significance (* or † denotes $p < .05$ for a treatment-mediated effect or a genotype-mediated effect, respectively) using GraphPad Prism 6 (San Diego, California). Mechano- and thermosensitivity were analyzed using the paired student t test.

Results

Generation of PD-1 mutant rats (PD-1^{m/m}) using CRISPR/Cas9

Based on the known crystal structures of mouse and human PDCD1 genes, both alone and in combination with PD-L1 and pembrolizumab, 2-guide RNAs (gRNAs) were generated targeting a segment of exon 2 in *R. norvegicus* (NC_005108.4; Reference Rnor 6.0 Primary Assembly) encoding the Ig domain (Figs. 1A–C). The extracellular domain containing the in-frame deletion (amino acids 30–140) has been shown to be critical in mediating PD-1/PD-L1 binding (Reddy et al., 2019). Thus, deletion of the area indicated in exon 2 (Figure 1C—bold, Figure 1D) would be

expected to inhibit both the ligand-binding and amino acid interactions required within the PD-1/PD-L1 or PD-L2 heterodimer interface for polypeptide interaction. The deleted sequence includes the core binding sequence for PD-L1 and pembrolizumab based on crystallographic and functional data (purple highlight) (Horita et al., 2016). As indicated in Figure 1E, this region demonstrates considerable homology between rats, mice, and man. Presence of the mutant allele (“m”) was verified using 2 independent sets of genetic primers (Figure 2A) to determine individual genotypes (Figure 2B). PD-1^{+/m} rats were mated, producing progeny at the expected Mendelian ratios for each of the expected genotypes (25% wild-type, 50% heterozygous, 25% homozygous) demonstrating a lack of embryonic lethality in PD-1^{m/m} animals. Sanger sequencing of genomic DNA from each of the genotypes confirmed the expected targeting of gRNAs as shown in Figure 3, resulting in an in-frame deletion of 153 bp (51 aa) in exon 2. Listed genotyping, gRNA, and sequencing primers are given in Supplementary Tables 1 and 2. Sequencing PD-1 genomic DNA within our SD colony stock demonstrated results comparable with that reported in NCBI reference data.

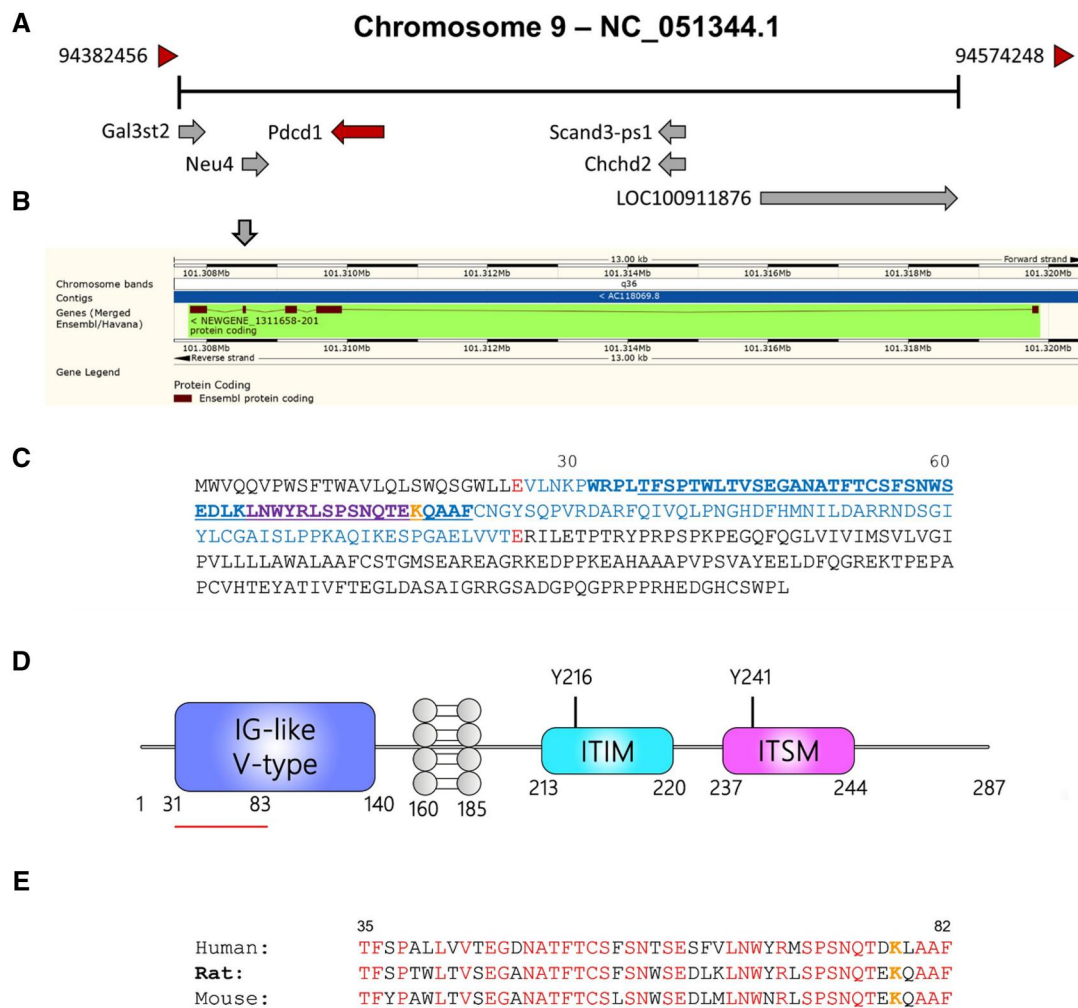


Figure 1. Modification of rat PDCD1 (PD-1) gene. A, Overview of the PDCD1 gene on rat chromosome 9. B, Detailed structure of rat PDCD1 gene highlighting modified exon 2. C, Amino acid sequence of the *R. norvegicus* PD-1 gene with exon 2 highlighted in blue. Amino acids indicated in red represent shared codons between exons 1, 2, and 2/3. The bolded sequence represents the region of induced deletion. The sequence highlighted in purple represents the identified core binding sequence for PD-L1/pembrolizumab based on crystallographic and functional data (Horita et al., 2016). The full protein length consists of 287 amino acids. Deletion of lysine 78 (orange) results in the nullification of PD-L1/L2 binding. The underlined sequence identifies the homology alignment shown in (D). D, Schematic of PD-1 binding domains with the region of deletion. E, Amino acid sequence alignment with a degree of conservation of region deleted in PD-1 compared with related species. Conserved amino acids are shown in red (critical lysine residue is indicated in orange).

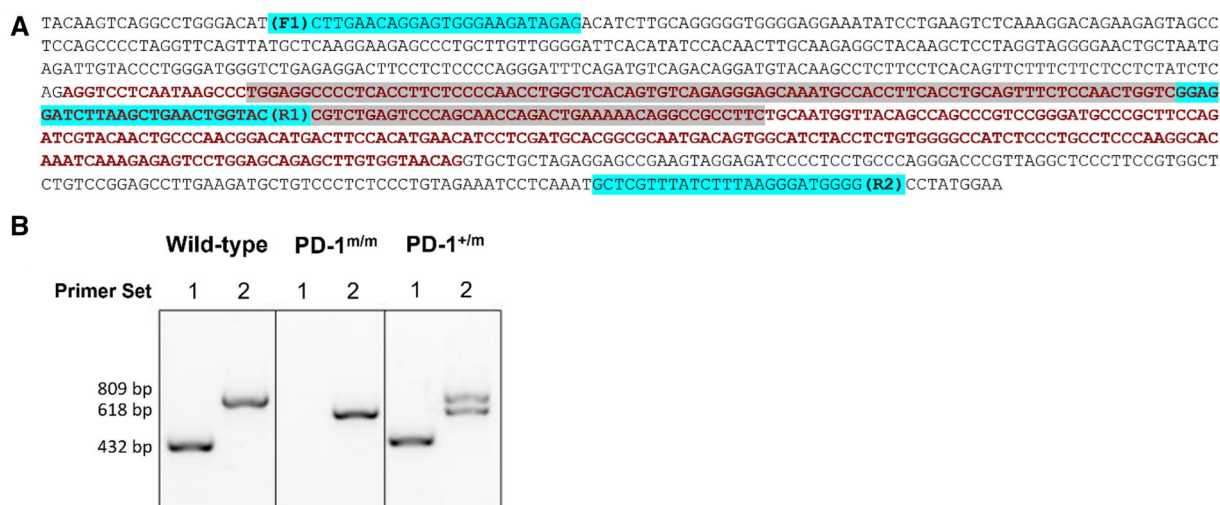


Figure 2. Genomic analysis of the rat *PDCD1* gene. A, Exon 2 (red) and surrounding sequence of the rat *PDCD1* gene. Blue highlight—sequencing primers utilized (F1: forward primer 1/2, R1: reverse 1, R2: reverse 2). The extent of the induced deletion is highlighted in gray. B, Example of PCR results obtained as a function of genotype. Primer set no. 1 (for sequences, see Supplementary Table 1) denotes a single amplicon of 432 bp for wild-type and heterozygous (PD-1^{+m}) rats, with the absence of a band in homozygous (PD-1^{m/m}) animals. Primer set no. 2 denotes a single band of 809 bp for wild-types, a band of 618 bp for homozygous mutants, with 2 separate bands of 618 and 809 bp for heterozygous animals. Using primer set no. 2, heterozygous animals are easily identified as they produce 2 distinct bands, whereas homozygous wild-type or PD-1^{m/m} animals display a single band. Prior electropherogram results were verified using LabChip GX (PerkinElmer; Waltham, Massachusetts) at TCP (data not shown).

PDCD1 Coding Domain Sequence

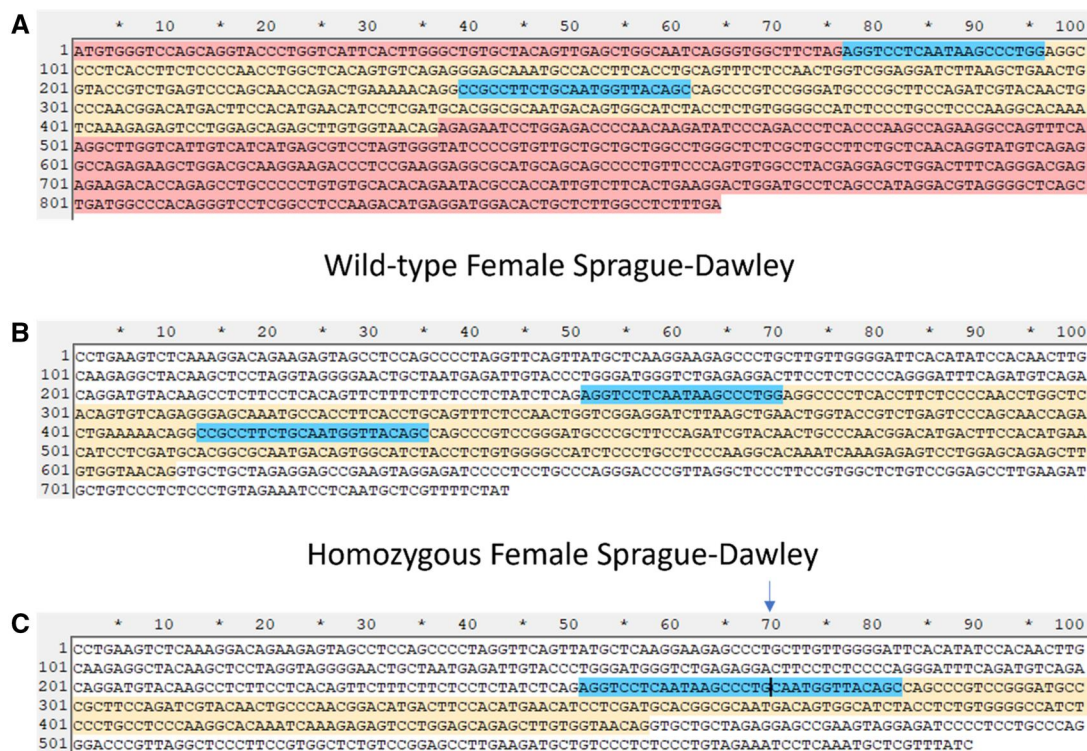


Figure 3. Genomic modification of *PDCD1* locus. A, Nucleotide coding sequences of the rat *PDCD1* gene. The segment corresponding to exon 2 is indicated by the yellow highlight. The relative position of CRISPR guides used to modify rat *PDCD1* coding domain sequence is indicated in blue. B, Genomic sequencing of wild-type littermates. C, Genomic sequencing of homozygous PD-1^{m/m} rats demonstrating in-frame deletion of 153 bp within the domain of the 2 gRNA sequences as indicated by the arrow and black line.

Sequencing of PD-1^{m/m} progeny demonstrated excision of a 153-bp segment between gRNA sequences as shown in Figure 3C. This deletion resulted in an in-frame removal of 51 amino acids

within the amino-terminal component of the IgG-like extracellular domain; thus, removing the extracellular ligand interaction motif while retaining transmembrane and intracellular

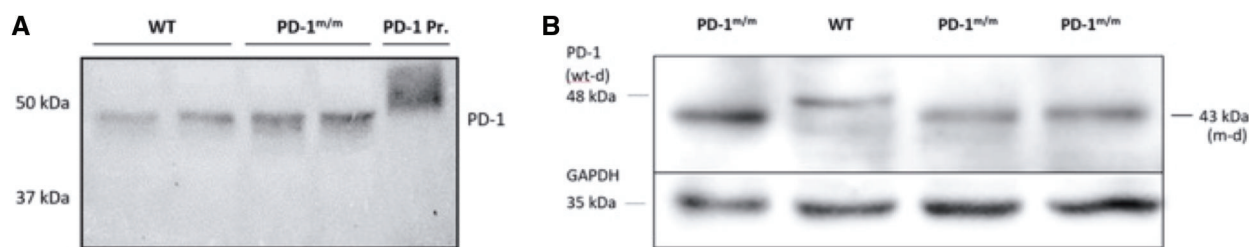


Figure 4. The molecular weights of glycosylated and deglycosylated PD-1 protein from wild-type and PD-1^{m/m} rats (A) PD-1 was visualized at approximately 50 kDa using an anti-PD-1 antibody. Purified PD-1 protein from rats (PD-1 Pr.) appears at the approximately 55 kDa mark due to the Fc tag (lane 5; obtained commercially). B, Chemically deglycosylated samples of PD-1 spleen in wild-type versus PD-1^{m/m} animals, showing a difference in molecular weight as a result of exon 2 deletion. Deglycosylated wild-type band (wt-d) at 48 kDa and deglycosylated PD-1 mutant proteins (m-d) are indicated.

immunoreceptor tyrosine-based inhibitory motif and immunoreceptor tyrosine-based switch motif signaling.

Expression of PD-1 protein in wild-type and PD-1^{m/m} rats

To determine how this induced mutation altered PD-1 expression in PD-1^{m/m} animals compared with wild-type animals, thymic extracts were prepared and examined by SDS/PAGE. Based on its amino acid sequence, murine PD-1 exhibits a molecular weight of 31.9 kDa. However, its relative mobility as documented in prior studies is approximately 37–55 kDa by SDS-PAGE (Martins et al., 2022). This range of apparent molecular weights is in large measure due to glycosylation of the peptide backbone as well as ubiquitination (Li et al., 2016). Such modifications can obscure changes to the peptide backbone by SDS-PAGE as shown in Figure 4A (antibody specificity verified using purified Fc-tagged rat PD-1 as shown in lane 5; obtained commercially). As such, chemical deglycosylation of PD-1 was employed as shown in wild-type and homozygous PD-1^{m/m} rats in Figure 4B, with the change in apparent molecular weight demonstrating the effects of deglycosylation and deletion of amino acids in the PD-1 mutant.

Female and male PD-1^{m/m} animals exhibit elevated mortality not seen in wild-type or PD-1^{+/+} rats

Untreated PD-1^{m/m} animals between the ages of 8–12 weeks exhibited an elevated mortality rate of approximately 8% compared with PD-1 heterozygous or wild-type littermates. Necropsy revealed no definitive gross observations aside from muscle wasting with diminished visceral white adipose tissue and reduced body weight. As such, livers and spleens of moribund wild-type and mutant animals were stained for histological changes (Supplementary Figure 1). Focal areas of inflammation were noted in the liver of PD-1^{m/m} animals, similar to observations seen in untreated PD-1^{-/-} mice (Metushi et al., 2015). A poorly defined marginal zone in the spleen segregating lymphoid follicles from the periarteriolar lymphoid sheaths was also observed in PD-1^{m/m} animals compared with wild-type animals. Animals that survived beyond this period demonstrated normal serum ALT levels and were utilized for subsequent drug treatment studies.

Female PD-1^{m/m} animals do not exhibit increased thermal or mechanical hypersensitivity compared with wild-type animals

Prior descriptions of mechanical allodynia and thermal and mechanical hypersensitivity have been reported in mice lacking PD-1 (Chen et al., 2017), PD-1^{m/m} rats were examined to determine if they exhibited altered thermal or mechanical

hypersensitivity. Examination using standard von Frey filament and hot plate assays in PD-1^{m/m} female rats exhibited no significant differences compared with wild-type females for either measure (Supplementary Figure 2).

Male and female PD-1^{m/m} rats treated with amodiaquine exhibit phenotypic differences when compared with similarly treated wild-type animals

As described previously, female PD-1^{-/-} mice treated with the anti-malarial drug, amodiaquine, display increased serum ALT levels together with the portal vein infiltration of lymphocytes in the liver following 3 weeks of treatment (Metushi et al., 2015). In contrast, male PD-1^{-/-} mice treated with amodiaquine did not develop liver injury; covalent binding of amodiaquine was less in males compared with females, and there was no evidence of liver infiltrates. As a first step toward examining these effects in rats and similarities within these respective models, SD PD-1^{m/m} rats were treated with amodiaquine over a similar dosing regimen to determine their propensity for idiosyncratic drug-induced liver injury as seen in our prior murine model. Male and female wild-type and PD-1^{m/m} rats were treated orally with amodiaquine (0.2% w/w in rodent meal) for 3 weeks as described previously. This period corresponded to the maximum treatment period prior to observing features of distress in female PD-1^{m/m} treated rats (Sotocinal et al., 2011). Similar effects were observed in male PD-1^{m/m}; however, the severity and spectrum of effects were not as pronounced. In most animals, clinical signs included hunched posture, respiratory distress, weight loss, decreased activity, and piloerection. Again, these features were found to be more pronounced in frequency and severity in females compared with male PD-1^{m/m} rats. By 3 weeks of treatment, male and female amodiaquine-treated PD-1^{m/m} rats exhibited substantial elevations in serum ALT levels compared with amodiaquine-treated wild-type littermates (Figure 5). This provides strong evidence that inhibition of PD-1 ligand binding within the PD-1 ectodomain is responsible for promoting amodiaquine-induced liver injury.

Following the 3-week dosing, the spleen, inguinal lymph nodes, liver, and thymus were removed from rats for analysis. Although no gross changes in thymus or liver weights were observed in male or female PD-1^{m/m} amodiaquine-treated animals compared with controls (Supplementary Figure 3), the size and weight of the spleen and inguinal lymph nodes were found to be increased in male and female PD-1^{m/m} amodiaquine-treated rats compared with controls (Figure 6). These differences achieved statistical significance by ANOVA as a function of genotype in amodiaquine-treated PD-1^{m/m} female rats; this increase remained a trend in the treated PD-1^{m/m} males. The observed differences in thymic versus splenic/lymph node response are

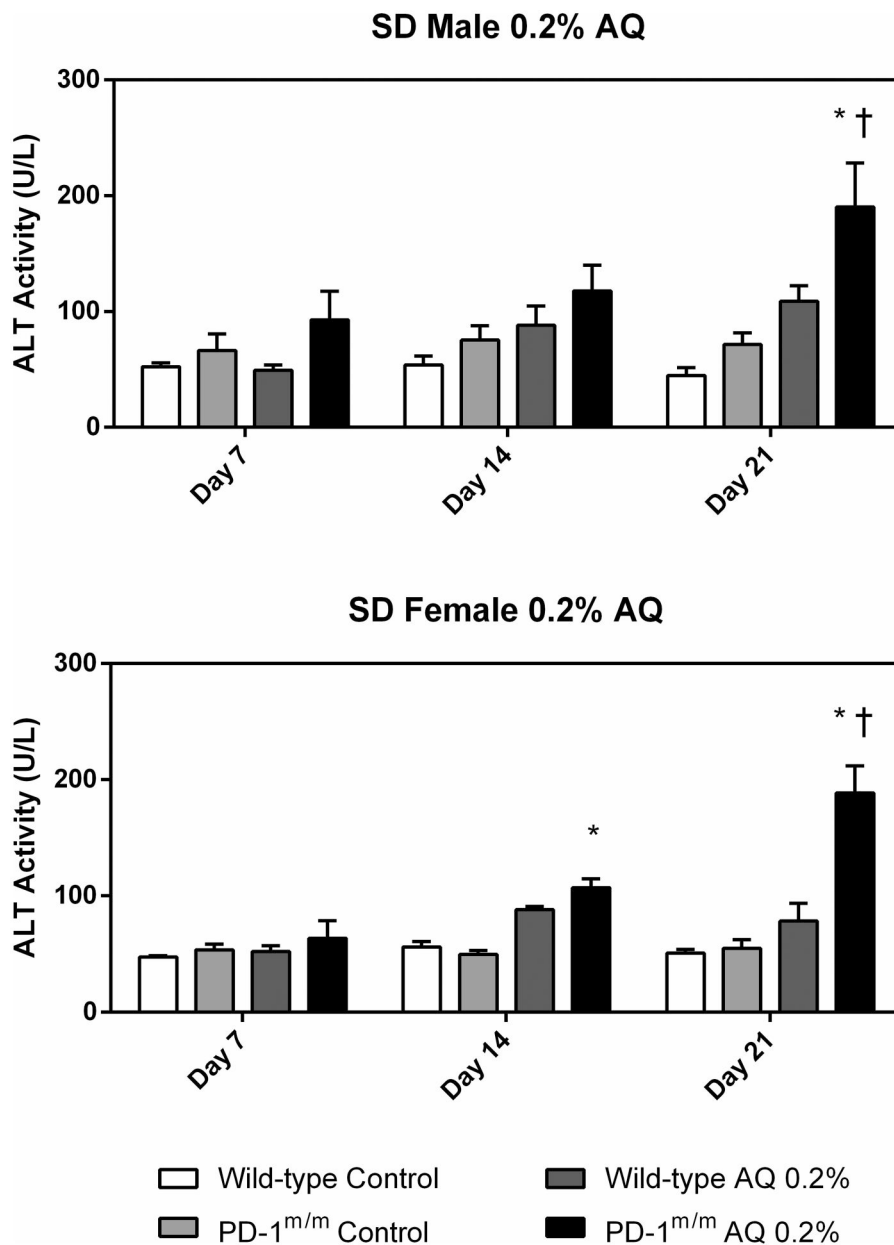


Figure 5. Serum ALT levels in the presence and absence of amodiaquine (AQ) treated and untreated PD-1^{m/m} rats and controls. Exposure to amodiaquine led to significant increases in ALT levels in PD-1^{m/m} rats compared with wild-type littermates. ALT elevations observed in wild-type animals were not significant. Data are represented as mean \pm SEM with statistical significance assessed using a 2-way ANOVA with Tukey's multiple comparisons test ($n=3$ per group), * $p < .05$ for treatment-mediated effects (genotype as a function of treatment); † $p < .05$ for genotype-mediated effects between wild-type and PD-1^{m/m} animals (treatment as a function of genotype).

consistent with differences in potential toxicant exposure due to lymphatic drainage (Trevaskis et al., 2015).

To investigate this in more detail, liver and spleen samples were examined for their pattern of PD-1 expression. As shown in Figures 7 and 8, focal areas of fibrosis and inflammation were observed in regions proximal to the central vein in PD-1^{m/m} rats but not in wild-type littermates. Consistent with this, these regions are associated with clusters of PD-1⁺ cells and hepatocyte degeneration. Similarly, within the spleen, although wild-type animals exhibited well-organized germinal and marginal zones, PD-1^{m/m} rats treated with amodiaquine exhibited substantial disorganization of these structures with wide dissemination of PD-1⁺ cells. Areas of extramedullary hematopoiesis were also

noted. Similarly in the inguinal lymph nodes (Figure 7), the follicular structure was not clearly defined in the treated male and female PD-1^{m/m} animals compared with controls.

To determine if any leukocyte class-specific changes were induced as a result of PD-1 modification, levels of T and B lymphocytes, monocytes, macrophages, antigen-presenting cells, and NK cells were examined by FACS analysis as shown in Supplementary Figure 4. With few exceptions, and despite a noted overall increase in lymphocyte infiltration into organs, no significant class-specific changes in the above cellular populations were observed (Supplementary Figs. 5 and 6). However, multiple focal inflammatory infiltrates specific to treated male and female PD-1^{m/m} livers were observed.

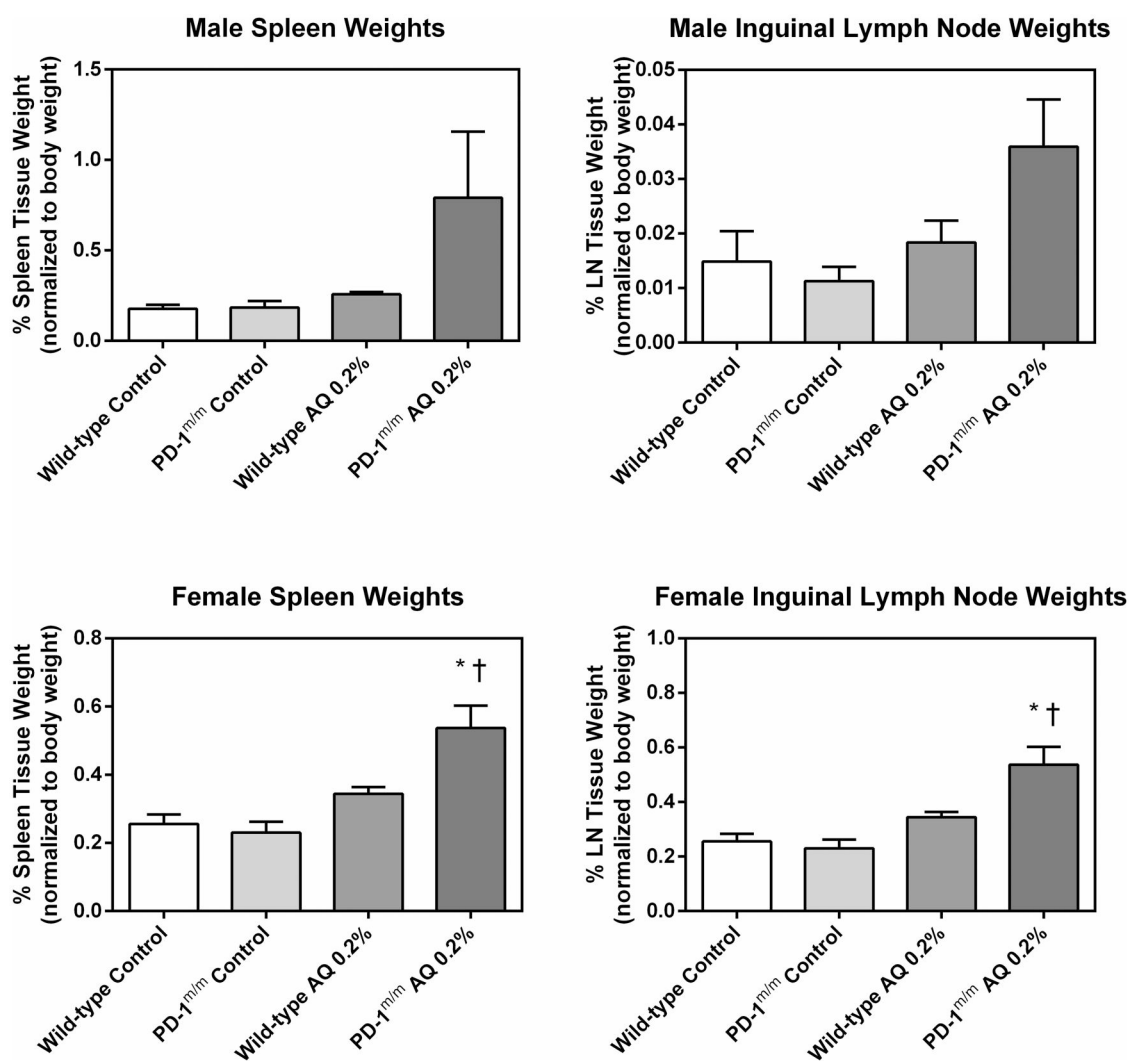


Figure 6. Weight of the spleen and inguinal lymph nodes following 3 weeks of amodiaquin (AQ) treatment in male and female PD-1^{m/m} rats. Although total weight changes in spleens and inguinal lymph nodes in males did not achieve significance, a clear trend toward increase was observed in PD-1^{m/m} AQ-treated animals compared with wild-type littermates. In contrast, the weights of spleens and lymph nodes in female PD-1^{m/m} rats were significantly increased relative to wild-type littermates. Data are normalized to body weight at endpoint. The data are shown as mean ± SEM, with statistical significance assessed using a 2-way ANOVA with Tukey's multiple comparisons test ($n = 3$ per group), $*p < .05$ for treatment-mediated effects (genotype as a function of treatment); $\dagger p < .05$ for genotype-mediated effects between wild-type and PD-1^{m/m} animals (treatment as a function of genotype).

Discussion

The objective of this study was to develop a rat with impaired PD-1 function similar to the PD-1^{-/-} mouse. If successful, this rat could be used to study IDRs caused by drugs for which the mouse is not a good model. IDRs pose a significant problem as they represent a significant source of patient morbidity and mortality while also increasing the risk of drug failure during and following development (Cho and Uetrecht, 2017). Although the detailed causal mechanisms of many IDRs remain unclear, there is strong evidence to suggest that most are immune mediated. However, given the diverse nature of drug entities capable of triggering IDRs and the varied cellular entry points and mechanisms capable of triggering immune-mediated responses, the specific features of individual IDRs are likely to be distinct. As such, animal models provide 1 important tool in evaluating multiorgan responses to clinical IDRs, despite the difficulties of these models in recapitulating all aspects of human clinical drug responses (Ng et al., 2012). In particular, rats and mice represent widely

accessible models and exhibit significant and useful differences in immune response and physiology (Bryda, 2013). Although mice have historically possessed notable advantages with respect to inbreeding and the maturity of its gene modification technologies (Parker et al., 2014), the advent of genome-editing technologies such as CRISPR have allowed a facile route toward modifications in a variety of organisms (Carroll and Frakt, 2017; Hsu et al., 2014). This potentially allows for the utilization of rat models in which a number of physiologic and drug metabolism aspects are better characterized compared with mice.

Although the major role of PD-1 is believed to be related to immune tolerance, PD-1/PD-L1 have been shown to regulate elements of nociception in mice. PD-1 blockade or PD-L1 neutralization in mice has been shown to result in increased thermal and mechanical hypersensitivity (Chen et al., 2017). Another study has also demonstrated that PD-1-deficient mice and PD-1 blockade led to a reduction in gamma-aminobutyric acid (GABA)ergic neurotransmission, which resulted in impaired GABA-mediated

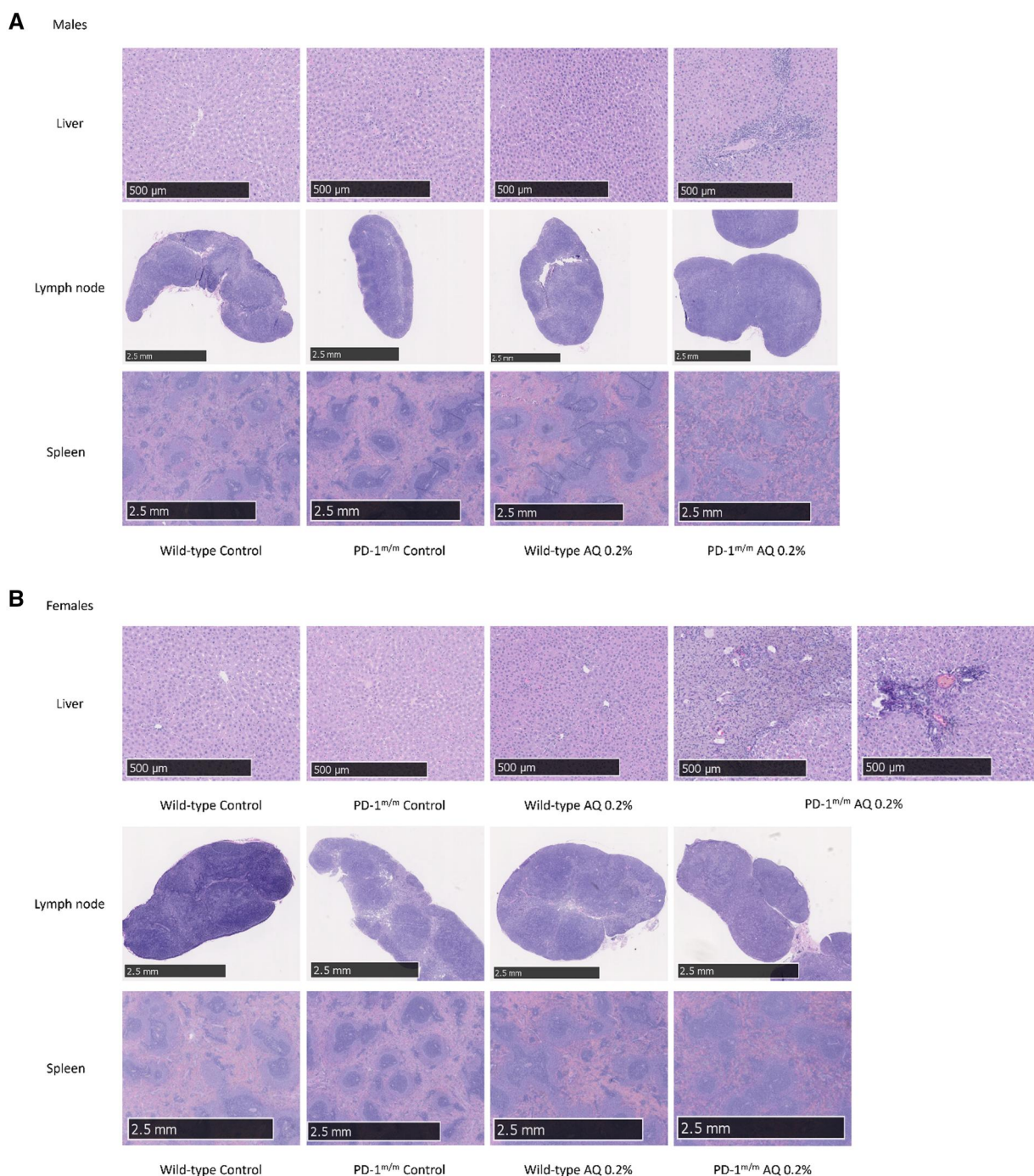


Figure 7. Overview of histology of liver, inguinal lymph nodes, and spleen at endpoint. Representative H&E images from control and amodiaquine-treated wild-type and PD-1^{m/m} males (A) and females (B) rats are shown. A, Sections of the liver (top); inguinal lymph nodes (middle) and spleen (bottom) are shown. In amodiaquine-treated PD-1^{m/m} versus wild-type animals, both male and female rats exhibited diffuse hepatitis with depletion of hepatocytes in conjunction with active necrosis and mononuclear leukocyte infiltrates in the liver. In the spleen, expansion of white pulp is observed with disorganization of marginal zones and lack of visible T-zone. Lymph nodes also show similar infiltrates. B, Similar pathology is observed in female AQ-treated PD-1^{m/m} rats versus AQ-treated controls. Sections from individual animals are shown and graded in [Supplementary Figure 7](#).

pain inhibition and anesthesia (Jiang et al., 2020). Although PD-1 plays an important role in the inhibition of hyperalgesia in mice, the same effects were not observed in the PD-1^{m/m} rats. This could be a result of species- and strain-related differences. It is also conceivable that the presence of a truncated PD-1 could still elicit its analgesic effects. However, the understanding of PD-1 in pain modulation is novel and will require additional studies to fully elucidate the mechanism of PD-1 in nociception (Nishimura

et al., 2001; Wang et al., 2010). In PD-1-deficient mice, the phenotype of the immune-mediated effects is strongly influenced by the strain of mice used. Dilated cardiomyopathy can be observed in PD-1 deficient mice on a BALB/c background without inflammation in the hearts, whereas hearts of PD-1-deficient mice on an MRL background were heavily infiltrated by lymphocytes and myeloid cells. PD-1 signaling is an important factor in the regulation of immune-mediated effects and we have previously

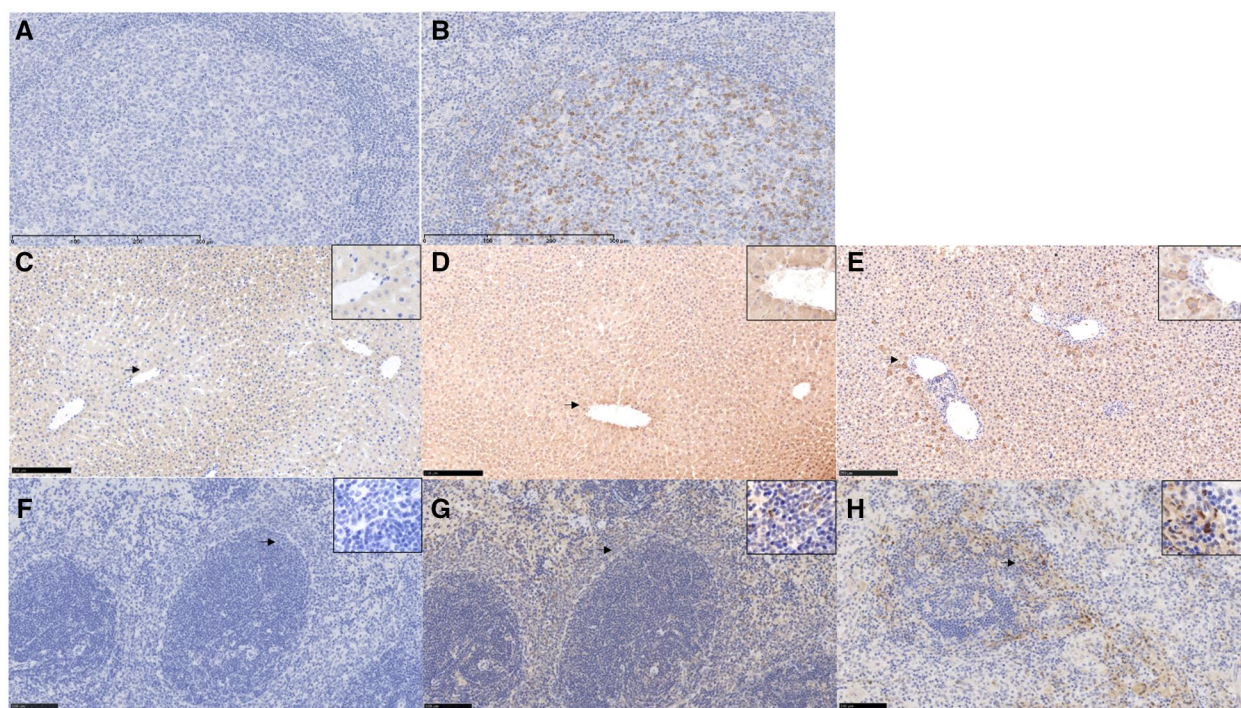


Figure 8. Analysis of PD-1 staining in wild-type and PD-1^{m/m} rats. A and B, Human tonsil, which was used as the tissue of choice for staining of PD-1 as PD-1 has a high expression and distribution in the T cells and a small subset of B cells in the human tonsil (Iwai et al., 2002). (A) Primary antibody negative control, (B) stained tissue sample (scale bar represents 300 μm). C–E, PD-1 rat livers on day 21. Insets regions are indicated by the arrow. (C) Primary antibody negative control, (D) wild-type littermate, and (E) PD-1^{m/m} rat (scale bars represent 250 μm). F–, PD-1 rat spleens on day 21. Insets regions are indicated by the arrow. F, Primary antibody negative control, (G) wild-type littermate, and (H) PD-1^{m/m} rat (scale bars represent 100 μm).

observed increased immune cell infiltration of the liver in untreated PD-1-deficient mice. Intra- and interspecies differences may result in the severity of effects seen with PD-1 modulation and may explain the mortality and clinical signs seen in untreated PD-1^{m/m} rats.

In recent years, immunologic progress in the area of cell-cell communication has focused attention on understanding the important role of immune modifiers such as PD-1 and CTLA-4 in self/non-self-recognition (Buchbinder and Desai, 2016; Intlekofer and Thompson, 2013). Previously, we developed an animal model of idiosyncratic drug-induced liver injury through the combined use of PD-1^{-/-} mice in conjunction with an anti-CTLA-4 antibody to examine mechanisms of IDRs (Metushi et al., 2015). The PD-1^{-/-} mouse model of idiosyncratic liver injury with amodiaquine and other drugs appears to closely represent the mechanism of drug-induced idiosyncratic liver injury in humans (Mak et al., 2018). Specifically, the dominant mechanism of injury in humans appears to be mediated by CD8⁺ T cells. The evidence for this includes the observation that most of the associations of HLA haplotypes with the risk of liver injury caused by specific drugs are MHC-I molecules, which bind to CD8 (Daly and Day, 2012). In addition, the liver histology of drug-induced liver injury is characterized by a mononuclear infiltrate dominated by CD8⁺ T cells (Foureau et al., 2015). PD-1 is expressed on T cells, and depletion of CD8⁺ T cells in the PD-1^{-/-} mouse model prevented the liver injury (Mak and Uetrecht, 2015b). Thus, it appears that, like idiosyncratic drug-induced liver injury in humans, the liver injury in the PD-1^{-/-} model is also mediated principally by CD8⁺ T cells. Immune checkpoint inhibition also increases the risk of liver injury caused by co-administered drugs in humans (Ribas et al., 2013); therefore, there are multiple lines of evidence to indicate that the mechanism of liver injury in the PD-1^{-/-} mouse

model is similar to the mechanism of idiosyncratic drug-induced liver injury in humans.

In the current study, we have attempted to extend these findings to a rat model of drug response using the CRISPR/Cas9 system. These prior studies highlighted the potential significance of bidirectional PD-1/PD-L1 signaling in regulating some aspects of the response (Han et al., 2020; Hudson et al., 2020; Wu et al., 2022). As a first step in delineating such effects, we sought to ablate the extracellular ligand binding domain from PD-1 while retaining potential intracellular signaling domains. Animals homozygous for this mutation, which targeted the same ectodomain interface modified by current clinical PD-1 antisera, demonstrate the significance of inhibiting the PD-1/ligand interface in regulating several aspects of the response to amodiaquine.

In experiments conducted with amodiaquine, an antimalarial drug that causes idiosyncratic drug-induced liver injury in humans, serum ALT levels were elevated, and inflammatory infiltrates were observed in the liver of amodiaquine-treated male and female PD-1^{m/m} rats. Moreover, the follicular structures within the spleen of these animals at week 3 appear to be less distinctive. These areas are rich in lymphocytes, macrophages, dendritic cells, and plasma cells (Cesta, 2006). Within the inguinal lymph nodes of the amodiaquine-treated PD-1^{m/m} animals, structurally intact lymphoid follicles were not observed when compared with control animals. Studies on PD-1^{-/-} mice on a C57BL/6 background demonstrate that they develop modestly, yet consistently, enlarged spleens, with elevated numbers of B cells and myeloid cells. These mice are phenotypically different from BALB/c PD-1^{-/-} mice where premature mortality occurs in 30% of the animals as a result of impaired function from an enlarged heart (Nishimura and Honjo, 2001). It is not well understood what cellular changes may be inferred from the

enlargement of the lymphoid tissues, but hyperactivation of the immune system and proliferation of T and B lymphocytes is a plausible reason for the presence of splenomegaly and lymphedema in the treated PD-1^{m/m} rats. Ultimately, PD-1 has been studied extensively in mice and humans, and there are inter- and intraspecies differences (Okazaki and Honjo, 2007).

The PD-1^{m/m} rat was generated to serve as a model for IDRs, which appear to develop amodiaquine-induced liver injury similar to treated PD-1^{-/-} mouse models. These effects are characterized by the delayed-onset presentation of elevated ALT levels with the presentation of inflammatory foci in the liver. Using CRISPR/Cas9, the developed rat model replicates many of the hallmarks of idiosyncratic drug-induced liver injury in humans indicating that one factor that prevents most patients from developing idiosyncratic amodiaquine-induced liver injury is immune tolerance, and these effects are regulated by modification of PD-1 ligand-binding. This model thus extends our ability to study mechanisms of IDRs, not only with respect to amodiaquine but also nevirapine-induced skin rash and clozapine-induced agranulocytosis. Although an anti-PD-1 antibody might achieve many of the same effects; in general, gene modifications usually provide a better reflection of the role of a specific protein.

Supplementary data

Supplementary data are available at *Toxicological Sciences* online.

Declaration of conflicting interests

The authors declared no potential conflicts of interest with respect to the research, authorship, and/or publication of this article.

Acknowledgments

The authors wish to acknowledge the contribution of Dr Lauryl Nutter, Joanna Joeng, and the Model Production staff at The Centre for Phenogenomics for assistance in the generation of genetically modified rats. Cas9-mediated rat production was funded by the Government of Canada through Genome Canada and Ontario Genomics (OGI-099). They would like to thank members from the Faculty of Pharmacy including Dr Robert Bonin and Maham Zain for lending equipment and expertise for behavioral analyses; Dr Andrew Elia and Dr Lily Zhou at the Princess Margaret Hospital/University Health Network for their histologic services and knowledge; Beth Binnington from the Canadian Blood Services for consultation and assistance; Dr Nitin Bhardwaj for necropsies at the Division of Comparative Medicine, University of Toronto; Brittany Licorish, Laura Kent, and Stacy Nichols for care and maintenance of the genetically modified rat colony at the Division of Comparative Medicine, University of Toronto; and Kyra Alam for her guidance and support. They would also like to thank Dr Anthony Hayes for his advice and interpretations of histopathology.

Funding

Canadian Institutes of Health Research; Pfizer Canada; the Ontario Graduate Scholarship; the Glaxo Wellcome-Drug Sunnybrook Drug Safety Clinic Graduate Student Fellowship.

References

- Bannon, A. W., and Malmberg, A. B. (2007). Models of nociception: Hot-plate, tail-flick, and formalin tests in rodents. *Curr. Protoc. Neurosci.* Chapter 8, Unit 8.9.
- Behringer, R., Gertsenstein, M., Nagy, K., and Nagy, A. (2014). *Manipulating the Mouse Embryo: A Laboratory Manual*. Cold Spring Harbor Laboratory Press, New York.
- Bonin, R. P., Bories, C., and De Koninck, Y. (2014). A simplified up-down method (SUDO) for measuring mechanical nociception in rodents using von Frey filaments. *Mol. Pain*. **10**, 26.
- Bouabe, H., and Okkenhaug, K. (2013). Gene targeting in mice: A review. *Methods Mol. Biol.* **1064**, 315–336.
- Bryda, E. C. (2013). The mighty mouse: the impact of rodents on advances in biomedical research. *Mo. Med.* **110**, 207–211.
- Buchbinder, E. I., and Desai, A. (2016). CTLA-4 and PD-1 pathways: Similarities, differences, and implications of their inhibition. *Am. J. Clin. Oncol.* **39**, 98–106.
- Carroll, A. E., and Frakt, A. B. (2017). Children's health must remain a focus in the recovery from Hurricane Harvey. *JAMA Pediatr.* **171**, 1029–1030.
- Canadian Council on Animal Care (CCAC) (2020). *Guide to the Care and Use of Experimental Animals*, Vol. 1, 2nd ed. Ottawa, Canada. Available at: https://ccac.ca/Documents/Standards/Guidelines/Experimental_Animals_Vol1.pdf. Revised April 2020.
- Cesta, M. F. (2006). Normal structure, function, and histology of the spleen. *Toxicol. Pathol.* **34**, 455–465.
- Chaplan, S. R., Bach, F. W., Pogrel, J. W., Chung, J. M., and Yaksh, T. L. (1994). Quantitative assessment of tactile allodynia in the rat paw. *J. Neurosci. Methods*. **53**, 55–63.
- Chen, G., Kim, Y. H., Li, H., Luo, H., Liu, D. L., Zhang, Z. J., Lay, M., Chang, W., Zhang, Y. Q., and Ji, R. R. (2017). PD-L1 inhibits acute and chronic pain by suppressing nociceptive neuron activity via PD-1. *Nat. Neurosci.* **20**, 917–926.
- Cho, T., and Uetrecht, J. (2017). How reactive metabolites induce an immune response that sometimes leads to an idiosyncratic drug reaction. *Chem. Res. Toxicol.* **30**, 295–314.
- Daly, A. K., and Day, C. P. (2009). Genetic association studies in drug-induced liver injury. *Semin. Liver Dis.* **29**, 400–411.
- Daly, A. K., and Day, C. P. (2012). Genetic association studies in drug-induced liver injury. *Drug Metab. Rev.* **44**, 116–126.
- Filipiak, W. E., and Saunders, T. L. (2006). Advances in transgenic rat production. *Transgenic Res.* **15**, 673–686.
- Foureaux, D. M., Walling, T. L., Maddukuri, V., Anderson, W., Culbreath, K., Kleiner, D. E., Ahrens, W. A., Jacobs, C., Watkins, P. B., Fontana, R. J., et al. (2015). Comparative analysis of portal hepatic infiltrating leucocytes in acute drug-induced liver injury, idiopathic autoimmune and viral hepatitis. *Clin. Exp. Immunol.* **180**, 40–51.
- Gertsenstein, M., and Nutter, L. M. J. (2018). Engineering point mutant and Epitope-Tagged alleles in mice using Cas9 RNA-Guided nuclease. *Curr. Protoc. Mouse Biol.* **8**, 28–53.
- Giancchetti, E., Delfino, D. V., and Fierabracci, A. (2013). Recent insights into the role of the PD-1/PD-L1 pathway in immunological tolerance and autoimmunity. *Autoimmun. Rev.* **12**, 1091–1100.
- Han, Y., Liu, D., and Li, L. (2020). PD-1/PD-L1 pathway: current researches in cancer. *Am. J. Cancer Res.* **10**, 727–742.
- Higdon, L. E., Lee, K., Tang, Q., and Maltzman, J. S. (2016). Virtual global transplant laboratory standard operating procedures for blood collection, PBMC isolation, and storage. *Transplant. Direct.* **2**, e101.
- Horita, S., Nomura, Y., Sato, Y., Shimamura, T., Iwata, S., and Nomura, N. (2016). High-resolution crystal structure of the

- therapeutic antibody pembrolizumab bound to the human PD-1. *Sci. Rep.* **6**, 35297.
- Hsu, P. D., Lander, E. S., and Zhang, F. (2014). Development and applications of CRISPR-Cas9 for genome engineering. *Cell* **157**, 1262–1278.
- Hudson, K., Cross, N., Jordan-Mahy, N., and Leyland, R. (2020). The extrinsic and intrinsic roles of PD-L1 and its receptor PD-1: Implications for immunotherapy treatment. *Front. Immunol.* **11**, 568931.
- Iannaccone, P. M., and Jacob, H. J. (2009). Rats!. *Dis. Model. Mech.* **2**, 206–210.
- Intlekofer, A. M., and Thompson, C. B. (2013). At the bench: Preclinical rationale for CTLA-4 and PD-1 blockade as cancer immunotherapy. *J. Leukoc. Biol.* **94**, 25–39.
- Iwai, Y., Okazaki, T., Nishimura, H., Kawasaki, A., Yagita, H., and Honjo, T. (2002). Microanatomical localization of PD-1 in human tonsils. *Immunol. Lett.* **83**, 215–220.
- Jee, A., Sernoskie, S. C., and Uetrecht, J. (2021). Idiosyncratic drug-induced liver injury: Mechanistic and clinical challenges. *Int. J. Mol. Sci.* **22**, 2954.
- Jiang, C., Wang, Z., Donnelly, C. R., Wang, K., Andriessen, A. S., Tao, X., Matsuda, M., Zhao, J., and Ji, R. R. (2020). PD-1 regulates GABAergic neurotransmission and GABA-mediated analgesia and anesthesia. *iScience* **23**, 101570.
- Li, C. W., Lim, S. O., Xia, W., Lee, H. H., Chan, L. C., Kuo, C. W., Khoo, K. H., Chang, S. S., Cha, J. H., Kim, T., et al. (2016). Glycosylation and stabilization of programmed death ligand-1 suppresses T-cell activity. *Nat. Commun.* **7**, 12632.
- Mak, A., Kato, R., Weston, K., Hayes, A., and Uetrecht, J. (2018). Editor's highlight: an impaired immune tolerance animal model distinguishes the potential of troglitazone/pioglitazone and tolcapone/entacapone to cause IDILI. *Toxicol. Sci.* **161**, 412–420.
- Mak, A., and Uetrecht, J. (2015a). The combination of anti-CTLA-4 and PD1^{-/-} mice unmasks the potential of isoniazid and nevirapine to cause liver injury. *Chem. Res. Toxicol.* **28**, 2287–2291.
- Mak, A., and Uetrecht, J. (2015b). The role of CD8 T cells in AMODIAQUINE-INDUCED liver injury in PD1^{-/-} mice cotreated with anti-CTLA-4. *Chem. Res. Toxicol.* **28**, 1567–1573.
- Malmberg, A. B., and Bannon, A. W. (2001). Models of nociception: Hot-plate, tail-flick, and formalin tests in rodents. *Curr Protoc Neurosci* **6**, 8.9.1–8.9.15.
- Martins, C., Silva, M., Rasbach, E., Singh, P., Itoh, Y., Williams, J. B., Statham, E., Meurer, A., Martinez, D. V., Brandenburg, A., et al. (2022). Distinct antibody clones detect PD-1 checkpoint expression and block PD-L1 interactions on live murine melanoma cells. *Sci. Rep.* **12**, 12491.
- Metushi, I. G., Hayes, M. A., and Uetrecht, J. (2015). Treatment of PD-1(-/-) mice with amodiaquine and anti-CTLA4 leads to liver injury similar to idiosyncratic liver injury in patients. *Hepatology* **61**, 1332–1342.
- Ng, W., Lobach, A. R., Zhu, X., Chen, X., Liu, F., Metushi, I. G., Sharma, A., Li, J., Cai, P., Ip, J., et al. (2012). Animal models of idiosyncratic drug reactions. *Adv. Pharmacol.* **63**, 81–135.
- Nishimura, H., and Honjo, T. (2001). PD-1: An inhibitory immunoreceptor involved in peripheral tolerance. *Trends Immunol.* **22**, 265–268.
- Nishimura, H., Nose, M., Hiai, H., Minato, N., and Honjo, T. (1999). Development of lupus-like autoimmune diseases by disruption of the PD-1 gene encoding an ITIM motif-carrying immunoreceptor. *Immunity* **11**, 141–151.
- Nishimura, H., Okazaki, T., Tanaka, Y., Nakatani, K., Hara, M., Matsumori, A., Sasayama, S., Mizoguchi, A., Hiai, H., Minato, N., et al. (2001). Autoimmune dilated cardiomyopathy in PD-1 receptor-deficient mice. *Science* **291**, 319–322.
- Okazaki, T., and Honjo, T. (2007). PD-1 and PD-1 ligands: From discovery to clinical application. *Int. Immunol.* **19**, 813–824.
- Parker, C. C., Chen, H., Fligel, S. B., Geurts, A. M., Richards, J. B., Robinson, T. E., Solberg Woods, L. C., and Palmer, A. A. (2014). Rats are the smart choice: Rationale for a renewed focus on rats in behavioral genetics. *Neuropharmacology* **76 Pt B**, 250–258.
- Parry, R. V., Chemnitz, J. M., Frauwirth, K. A., Lanfranco, A. R., Braunstein, I., Kobayashi, S. V., Linsley, P. S., Thompson, C. B., and Riley, J. L. (2005). CTLA-4 and PD-1 receptors inhibit T-cell activation by distinct mechanisms. *Mol. Cell. Biol.* **25**, 9543–9553.
- Pirmohamed, M., Naisbitt, D. J., Gordon, F., and Park, B. K. (2002). The danger hypothesis—Potential role in idiosyncratic drug reactions. *Toxicology* **181-182**, 55–63.
- Reddy, V., Mwangi, W., Sadigh, Y., and Nair, V. (2019). In vitro interactions of chicken programmed cell death 1 (PD-1) and PD-1 ligand-1 (PD-L1). *Front. Cell. Infect. Microbiol.* **9**, 436.
- Ribas, A., Hodi, F. S., Callahan, M., Konto, C., and Wolchok, J. (2013). Hepatotoxicity with combination of vemurafenib and ipilimumab. *N. Engl. J. Med.* **368**, 1365–1366.
- Sernoskie, S. C., Jee, A., and Uetrecht, J. P. (2021). The emerging role of the innate immune response in idiosyncratic drug reactions. *Pharmacol. Rev.* **73**, 861–896.
- Shao, Y., Guan, Y., Wang, L., Qiu, Z., Liu, M., Chen, Y., Wu, L., Li, Y., Ma, X., Liu, M., et al. (2014). CRISPR/Cas-mediated genome editing in the rat via direct injection of one-cell embryos. *Nat. Protoc.* **9**, 2493–2512.
- Sharma, A. M., Novalen, M., Tanino, T., and Uetrecht, J. P. (2013). 12-OH-nevirapine sulfate, formed in the skin, is responsible for nevirapine-induced skin rash. *Chem. Res. Toxicol.* **26**, 817–827.
- Sotocinal, S. G., Sorge, R. E., Zaloum, A., Tuttle, A. H., Martin, L. J., Wieskopf, J. S., Mapplebeck, J. C., Wei, P., Zhan, S., Zhang, S., et al. (2011). The rat grimace scale: a partially automated method for quantifying pain in the laboratory rat via facial expressions. *Mol. Pain.* **7**, 55.
- Tiegs, G., and Lohse, A. W. (2010). Immune tolerance: What is unique about the liver. *J. Autoimmun.* **34**, 1–6.
- Trevaskis, N. L., Kaminskas, L. M., and Porter, C. J. (2015). From sewer to saviour—Targeting the lymphatic system to promote drug exposure and activity. *Nat. Rev. Drug Discov.* **14**, 781–803.
- Uetrecht, J., and Kaplowitz, N. (2015). Inhibition of immune tolerance unmasks drug-induced allergic hepatitis. *Hepatology* **62**, 346–348.
- Wang, J., Okazaki, I. M., Yoshida, T., Chikuma, S., Kato, Y., Nakaki, F., Hiai, H., Honjo, T., and Okazaki, T. (2010). PD-1 deficiency results in the development of fatal myocarditis in MRL mice. *Int. Immunol.* **22**, 443–452.
- Wu, M., Huang, Q., Xie, Y., Wu, X., Ma, H., Zhang, Y., and Xia, Y. (2022). Improvement of the anticancer efficacy of PD-1/PD-L1 blockade via combination therapy and PD-L1 regulation. *J. Hematol. Oncol.* **15**, 24.